ANL/CMT/CP-96628

Resistivity of Bipolar Plate Materials at the Cathode Interface in Molten Carbonate Fuel Cells

T. D. Kaun, A. C. Schoeler, I. Bloom, M. Lanagan, and M. Krumpelt
Chemical Technology Division
Argonne National Laboratory
9700 South Cass Avenue
Argonne, IL. 60439

Paper will be presented at the 194th Meeting of the Electrochemical Society, Boston, Massachusetts, USA

November 1-6, 1998

DISCLAIMER

RESISTIVITY OF BIPOLAR PLATE MATERIALS AT THE CATHODE INTERFACE IN MOLTEN CARBONATE FUEL CELLS

Thomas D. Kaun, Annett C. Schoeler, Ira Bloom,
Michael Lanagan, and Michael Krumpelt

Electrochemical Technology Program,
Chemical Technology Division,
Argonne National Laboratory,
9700 South Cass Avenue, Argonne IL 60439

ABSTRACT

Measurements of oxide scale resistivity for prospective bipolar plate materials in the molten carbonate fuel cell (MCFC) are coupled with observations of microstructural/compositional change over time. This work searches for a compromise to the high corrosion rate of Type 316L and the high oxide scale resistance of Type 310S. We tested a group of materials having chromium content ranging from 16 to 31 wt%, including Nitronic 50 and NKK, a Ni-Cr-Fe alloy. Chromium content was found to be the primary determinant of oxide scale composition. In the MCFC cathode compartment, stainless steels generally formed a duplex structure with an inner Cr-rich layer and an outer, Fe-rich layer. The composition of the inner Cr-rich layer was related to the base alloy and had a controlling effect on scale resistivity. Oxide scale resistivity was measured for two electrolyte compositions: Li/K and Li/Na carbonates. Changes in the physical/mechanical properties (spallation/cracking) in the oxide scale of Type 316L provided an understanding of its resistivity fluctuations over time.

INTRODUCTION

The molten carbonate fuel cell (MCFC) promises to generate power with a high efficiency and low emissions for stationary power plants. Corrosion of the bipolar plates and current collectors is caused by the high operating temperature (650°C) and the highly aggressive molten salts of the electrolyte. This limits the lifetime of the MCFC significantly (1). The resistance of the oxide layer on the cathode side of the bipolar plate diminishes the MCFC performance and may constitute a significant voltage loss. Approximately 25% of the internal cell resistance could be attributed to an oxide layer that forms on stainless steel used for the bipolar plate and current collector.

Several authors have investigated the corrosion behavior of stainless steels and the electrical conductivity of the corrosion layers, which are formed under the severe corrosion conditions in MCFC (1-6). They found that low-alloyed stainless steels with chromium contents under 15% do not fulfill the life requirements necessary for current collectors because fast-growing oxide layers are formed (5). Comparing the rates of corrosion and resistances of Types 310S and 316L stainless steel indicated that Type 310S

exhibits a 50% lower rate of corrosion, but the resulting oxide scales have higher electrical resistances (200-250 $m\Omega*cm^2$) compared to Type 316L (50 $m\Omega*cm^2$).

Besides stainless steels, Inconel, Ni-Cr alloys, Ni-Fe alloys and NKK are candidate materials for bipolar plate materials (3,6-9). The state-of-the-art for large scale MCFCs is to use 316L as the bipolar plate with Ni cladding in combination with $(Li,K)_2CO_3$ electrolyte.

The approach of this paper is to relate the interfacial electrical resistance of different stainless steels (316L, 310S, Nitronic 50) and Ni-based alloys with oxide scale composition as a function of exposure time and chemical composition of the electrolyte. We have monitored the resistivity of a group of samples, which were exposed to laboratory oxidant using $(Li,K)_2CO_3$ and $(Li,Na)_2CO_3$ electrolytes at 650°C. Samples were removed periodically to correlate changes in microstructure and resistance. While the (Li,K)-carbonate electrolyte is commonly used in the MCFC, the (Li,Na)-carbonate electrolyte shows promise for improved cell stability and minimal segregation (10). It also has a higher ionic conductivity and is less volatile. The NiO dissolution rate is significantly reduced in the less acidic (Li,Na)-carbonate electrolyte (11).

EXPERIMENTAL

Materials

Three different stainless steels and a nickel-based alloy were exposed under simulated MCFC conditions at 650°C. The chemical compositions of the materials are given in Table I. A 62 mol%Li_2CO_3-38 mol%K_2CO_3 (Li,K) mixture and a 52 mol%Li_2CO_3-48 mol%Na_2CO_3 (Li,Na) mixture were separately used as the electrolyte.

Table I Chemical composition of the tested materials

	Composition in wt%			
Element	**316L**	**NITRONIC 50**	**310S**	**NKK**
Ni	10.0-14.0	11.5-13.5	19.4	44.9
Fe	68.9-61.9	61.0-51.9	55.3	24
Cr	16.0-18.0	20.5-23.5	25.3	30.1
C	0.03	0.06	NA	NA
Mn	2	4.0-6.0	NA	NA
Mo	2.0-3.0	1.5-3.0	NA	NA

NA=not applicable

Procedure

Metal sheet samples were cut and polished to obtain a flat and smooth surface. The metal samples were placed between nickel electrodes, which were in contact with the electrolytes (Figure 1). The sample arrangement was preheated for one hour at 650°C to immerse the electrolyte in the porous nickel electrode. The nickel electrode oxidized and formed NiO. The porous NiO represents the cathode in our experiment. The molten electrolyte creeps in the oxidized porous nickel, lithiates the NiO, and forms a thin layer on the surface. The metal samples are, therefore, exposed directly to the molten electrolyte.

Figure 1 Schematic of the sample arrangement for the corrosion test

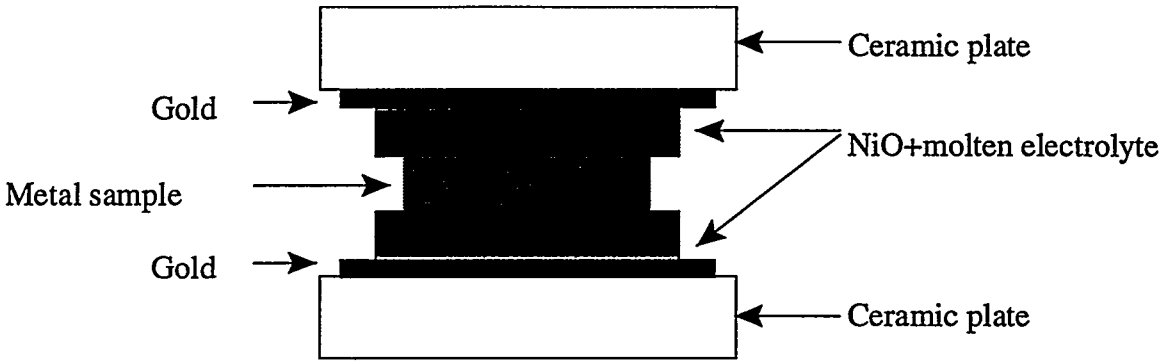

Corrosion tests were carried out in a cathodic environment (30 %CO_2/air) at 650°C for different exposure times. Afterwards, the samples were mounted, ground, polished, and subjected to microstructural measurements in order to characterize the corrosion behavior. Scanning electron microscopy (SEM) and energy dispersive X-ray spectrometry (EDX) were carried out on metallographic cross sections to determine the thickness and composition of the oxide scale.

Additionally, X-ray diffraction (XRD) measurements were undertaken. A special polishing device was used to remove definite amounts of the surface (≈5 μm) to determine the chemical composition of the oxide layer in the outer and inner area of the scale. After each "polishing" step, the phase distribution of the exposed surface was determined by XRD.

The electrical resistivity was also measured in the cathodic environment under MCFC conditions (650°C, 30 %CO_2/air) for various exposure times. It was possible to place 12 samples in a furnace specially designed for this purpose. A HP4338A milliohmmeter, which uses a four-wire measurement at 1 kHz, monitors the resistance of the samples. A computer is connected with a controller and measures the resistivity of each sample automatically. The samples were placed on an Al_2O_3 disk and connected with gold wires in series, as shown in Fig. 2. Periodically (about every 750 hr), some of the samples were removed from the furnace to determine the microstructural composition of the formed oxide scales.

Figure 2 Schematic of the sample arrangement for the electrical resistivity test

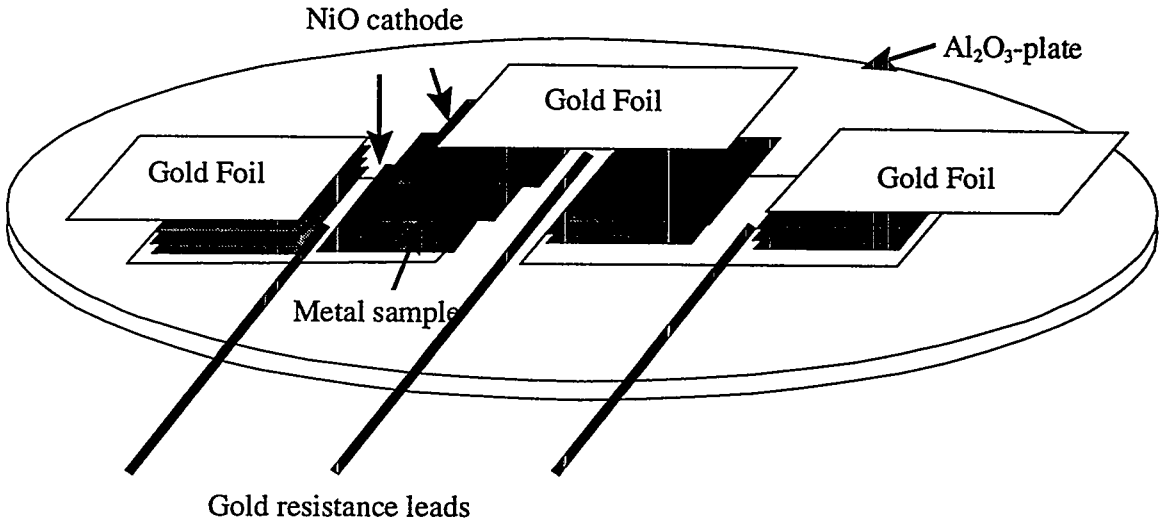

RESULTS AND DISCUSSION

Corrosion tests

The corrosion tests indicated that different alloys develop a wide range of oxide scale thicknesses and phases. The chromium content of the base metal is a key factor for the oxide scale thickness, as shown in Figure 3. Chromium clearly improves the corrosion resistance under MCFC conditions. While 316L (Cr content of 18 %) develops a relatively thick oxide scale of 25 μm after 1500 hours, the oxide scale of Nitronic 50 (Cr content of 22%) has a thickness of only 15 μm. The thickness of the oxide scale grows nearly linearly up to 2250 hours and reaches a plateau after long exposure times (3000 hours). The higher Cr content in 310S and NKK leads to slightly improved corrosion resistance compared to Nitronic 50 and 316L.

The chemical composition of the electrolyte also influences the oxide scale thickness. The scale thickness of all tested materials is slightly increased using (Li,K) electrolyte compared to (Li,Na) electrolyte. This can be explained by the lower Cr oxide solubility in (Li,Na) salt (9). Additionally, SEM micrographs indicated that the oxide scales of 316L, which was exposed under (Li,Na) salt, have a dense scale without visible large cracks or buckling. Some of the samples exposed to (Li,K) salt contain microcracks and buckling, as shown in Figure 4. Horizontal buckling and microcracks can be explained by the oxide growth. Oxides do not only grow in thickness, but also expand laterally, parallel to the metal surface; thus large compressive stresses occur in the scale, which cause microcracks and spallation.

Figure 3 Influence of the chromium content of the base metal on the oxide scale thickness for different exposure times and electrolytes

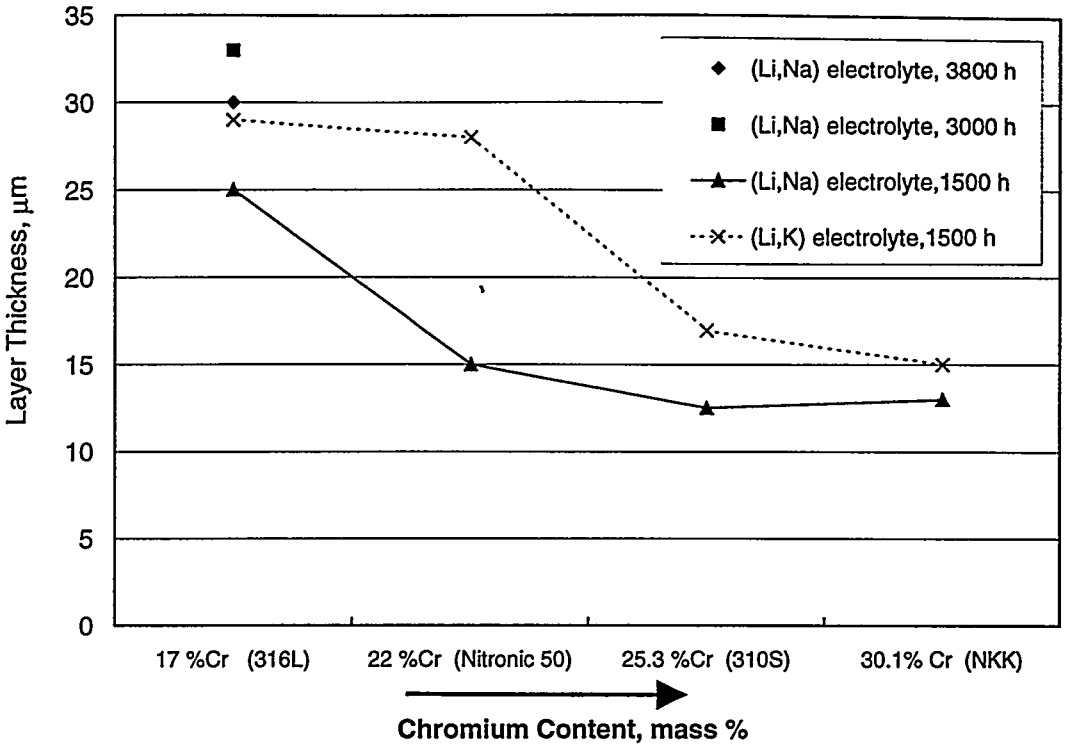

Figure 4 Scanning electron micrograph of 316L using (Li,K) electrolyte, exposure time: 2250 hours

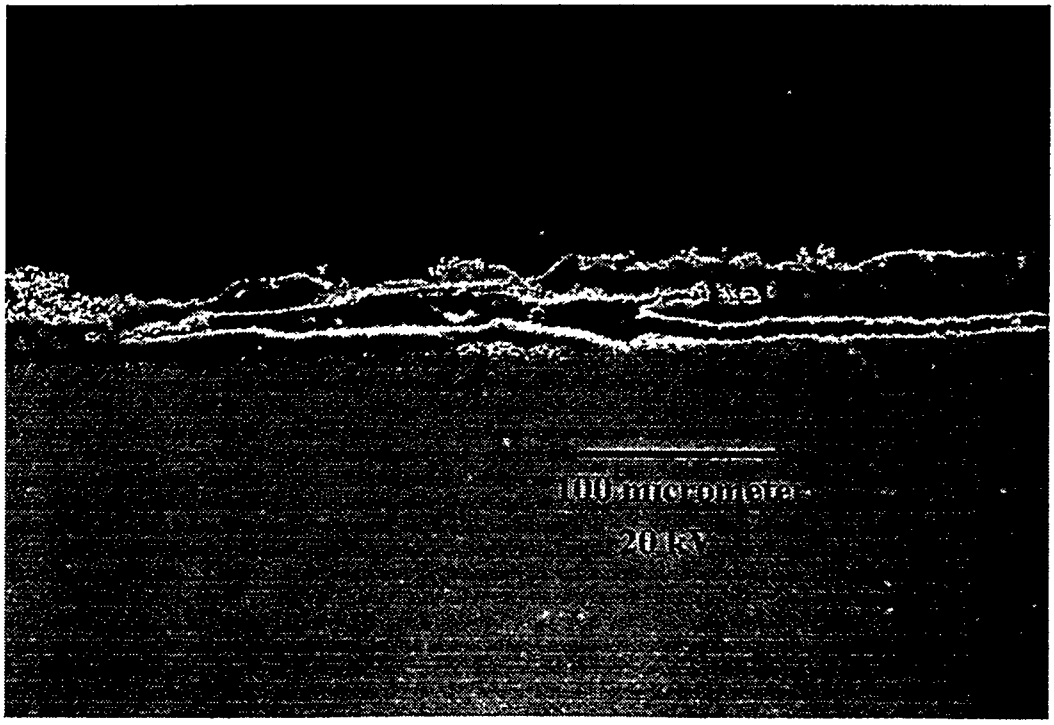

Both the XRD and EDX results showed that the outer layer of all analyzed materials consists of $LiFeO_2$, independent of the chromium content of the base metal and the electrolyte composition. In this outer layer the chromium content is very low, as shown in Figure 5. The nickel content in the outer layer is increased with raised nickel content of the base metal. The solubility of $LiFeO_2$ in the melt is very low, so that $LiFeO_2$ protects the metal from corrosion attack by the melt.

Additionally, we found slightly increased manganese content in the outer and inner layer of Nitronic 50. Other authors (5) determined the oxide scales of manganese-containing stainless steels with 8-20 wt% Mn. They detected a thin Li_2MnO_3 outer layer, Mn-containing $LiFeO_2$, and an inner spinel, where manganese is built in $[(Fe,Mn)Cr_2O_4]$. Further XRD investigations on Nitronic 50 will show if these oxide scale compositions are formed in this alloy.

Figure 5 Influence of the chromium content of the base metal on the element distribution in the outer layer under the (Li,K) and (Li,Na) electrolyte

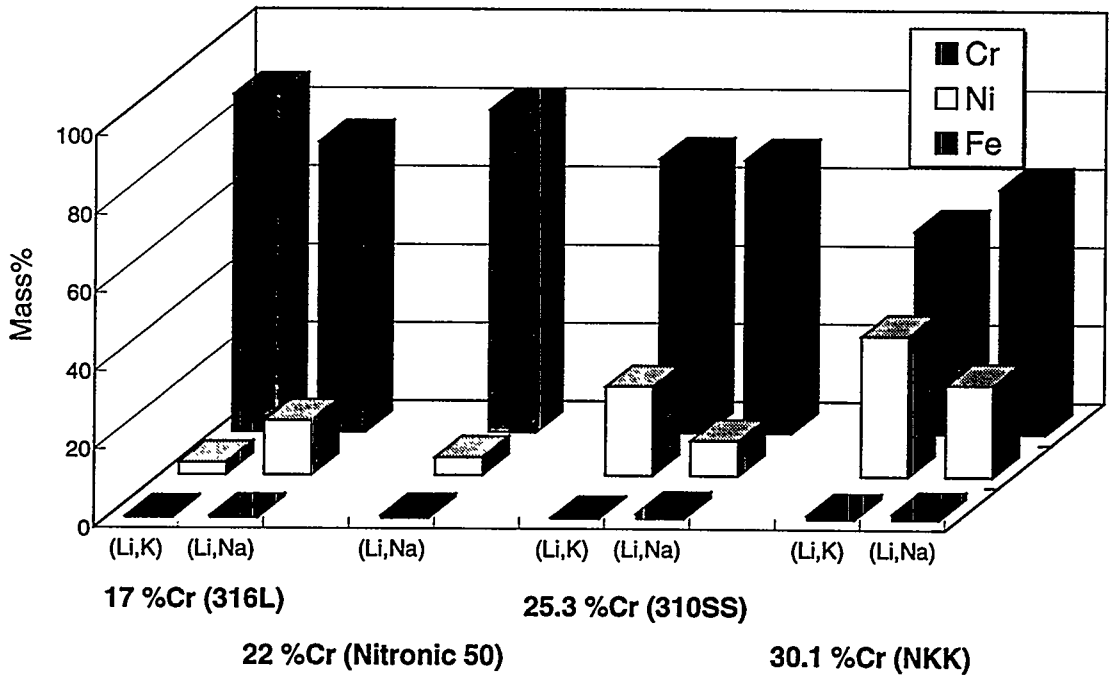

Figure 6 XRD pattern of the oxide scale of 316L under the (Li,Na) electrolyte

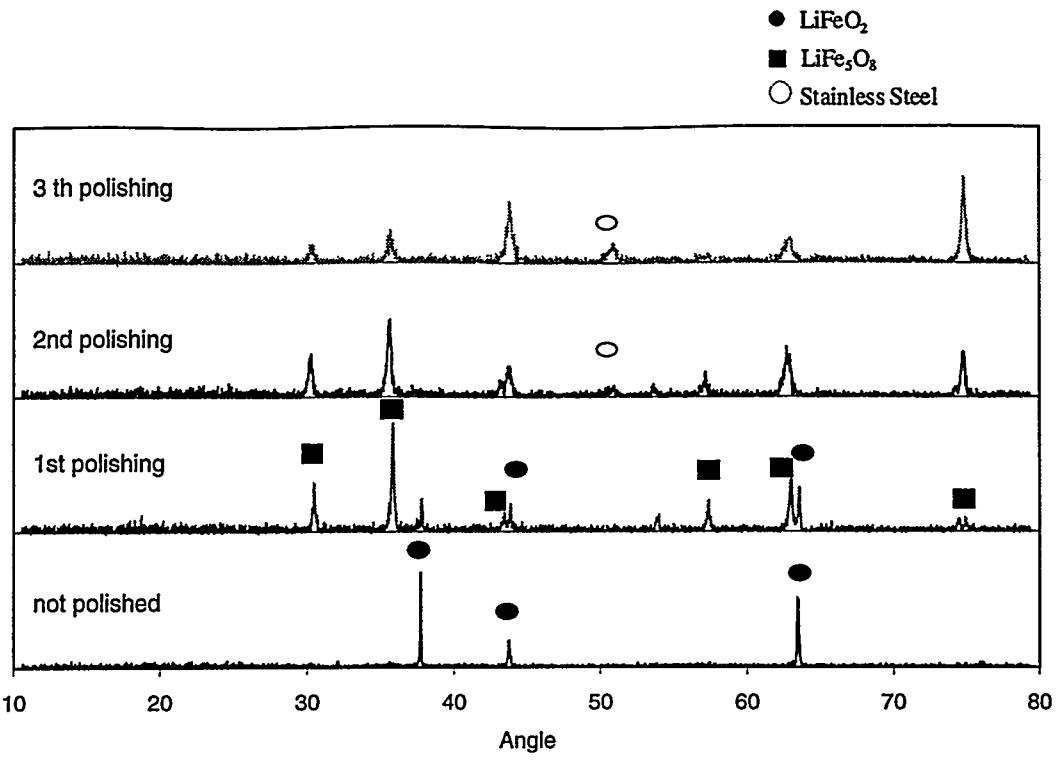

Figure 6 shows a typical XRD pattern through the oxide scales of 316L using (Li,K) electrolyte with an outer $LiFeO_2$ layer. For stainless steels, which contain between 16-18 %Cr, an outer layer is built from Fe_2O_3, which is formed in the first few hours (1). Marker experiments have shown that the outer layer mainly grows by outward iron diffusion (1):

$$Fe^{3+} + 2\,Li_2O \rightarrow LiFeO_2 + 3Li^+$$

Additionally, diffusion calculations indicated that the diffusion coefficient of iron in a high-alloyed stainless steel (Fe-19.9 at.%Cr-25 at.%Ni) is much greater than that of chromium in the temperature range from 650°C to 1100°C.

Unlike the outer layer, the structure of the inner layer is significantly influenced by the chromium content of the base metal. For example, 316L with a Cr content <20% forms a spinel structure such as $LiFe_5O_8$, which was observed by XRD (Figure 6). This corrosion product is formed under both tested electrolytes. For the 316L, a chromium-enriched inner layer was detected (Figure 7), but no $LiCrO_2$ could be detected with XRD. It is likely that chromium was built into the $LiFe_5O_8$ structure, or that $LiFe_5O_8$ and $FeCrO_4$ coexist.

Figure 7 EDX linescan through the oxide scale and the base metal 316L using (Li,Na) electrolyte, exposure time: 3800 hours

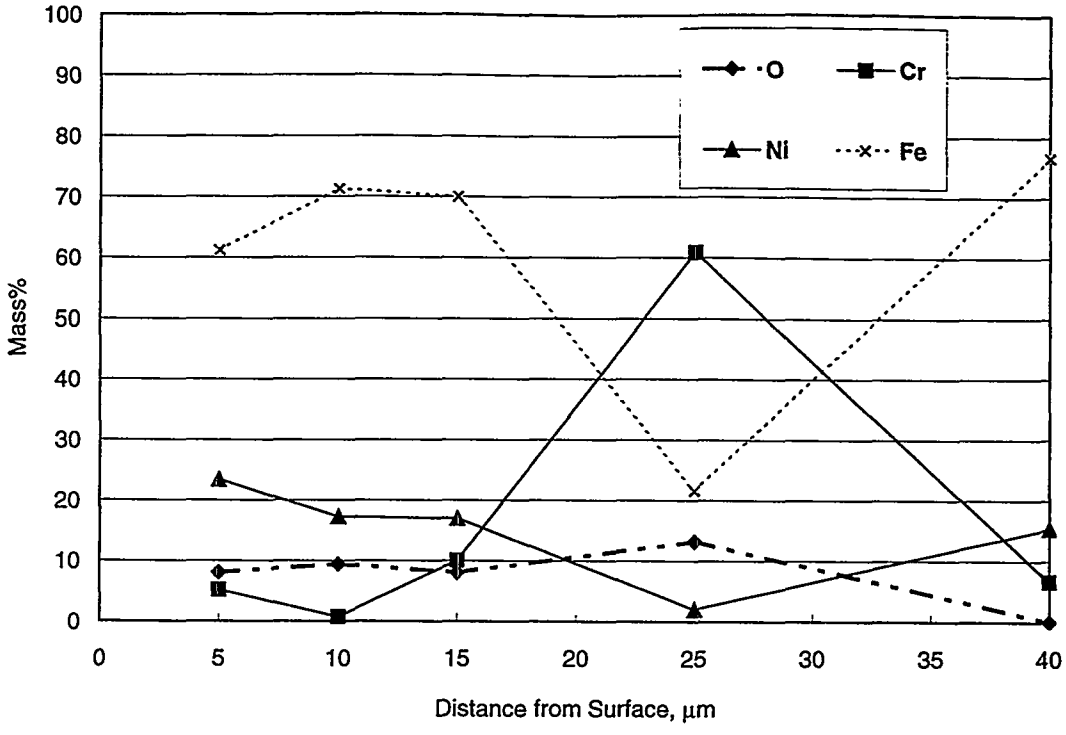

An increased chromium content >25% in stainless steels favors $LiCrO_2$ formation as an inner oxide scale. Neither 316L nor Nitronic 50 form $LiCrO_2$, but this was observed in XRD pattern for both chromium-rich alloys 310S and NKK. This oxide might be responsible for the better corrosion resistance of 310S and NKK because it limits the outward diffusion of iron and thus acts as a diffusion barrier (1). At higher temperatures $LiCrO_2$ is stable and prevents further corrosion under MCFC conditions (9).

The chemical composition of the electrolytes influences the oxide scale thickness, but not the structure of the oxide scale.

Electrical Resistance Test

As shown in Figures 8 and 9, the chromium content of the base metal influences the electrical resistivity significantly. A higher chromium content leads to higher resistivity values under both (Li,K) and (Li,Na) salt. The 316L and Nitronic 50 with chromium contents under 22% show low resistivities, while the resistivity of 310S and NKK with Cr contents >24% is twice as high, although the oxide scales are much thinner compared to 316L and Nitronic 50. Nitronic 50 with a relatively high chromium content has acceptable resistivity values (50-100 $m\Omega*cm^2$), which might be explained by the increased manganese content of 4 wt%. The modified oxides scales with increased Mn content may decrease the oxide scale resistivity.

Figure 8 Oxide scale resistivity of 316L, Nitronic 50, 310S, and NKK vs. time in the (Li,K) electrolyte

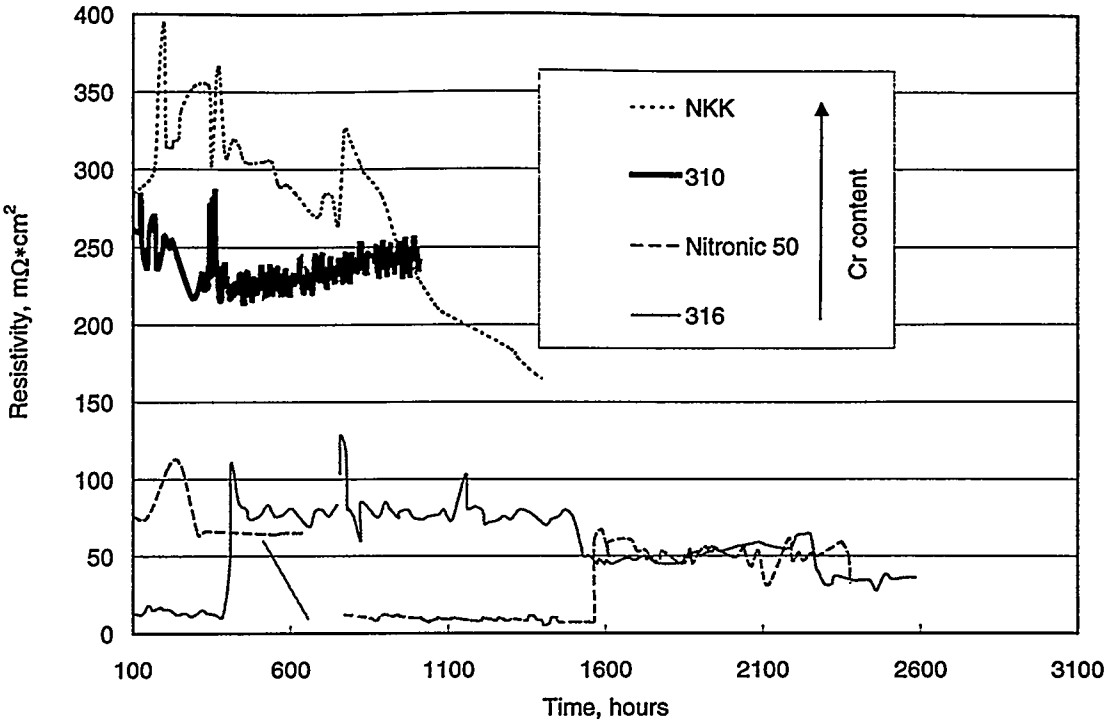

A key factor for the electrical resistivity seems to be the phase composition of the inner or intermediate oxide scales which are formed under MCFC conditions. The composition of the inner corrosion layer varies with chromium content of the base metal. Both 310S and NKK have an inner $LiCrO_2$ layer, which may lead to high resistivities. Additionally, we found porosity between the oxide scale and the base metal of NKK, which explains its rather high interfacial resistivity.

The oxide scale thickness does not play an important role in the electrical resistivity. For example, 316L and Nitronic 50 have a thicker oxide scale compared to 310S and NKK, but a lower electrical resistivity.

For 316L with the (Li,K) salt, the resistivity as a function of time (Figure 8) displays a saw-toothed pattern: first the resistivity reaches about 25 $m\Omega*cm^2$. After 500 hours, the resistivity increases to 130 $m\Omega*cm^2$ and then returns to about 25 $m\Omega*cm^2$. Others have observed this phenomenon. Horizontal buckling and porosity, a result of stresses related to oxide growth, can explain the fluctuations. After long exposure times, crystallite precipitations were observed, which have been determined to be Fe-Ni solid solutions. This is a result of a reaction between the NiO and the $LiFeO_2$ layer. Due to the formation of a solid solution of Fe-Ni, the resistivity decreases after long exposure times.

The electrical resistivity of 316L with the (Li,Na) electrolyte is slightly decreased compared to the (Li,K) electrolyte, especially in the first 1500 hours. The formation of a dense oxide scale without visible cracks or buckling could also explain the lower resistivity obtained with the (Li,Na) electrolyte. For Nitronic 50, no clear influence of the electrolyte is detectable.

Figure 9 Oxide scale resistivity of 316L and Nitronic 50 vs. time in (Li,Na) electrolyte

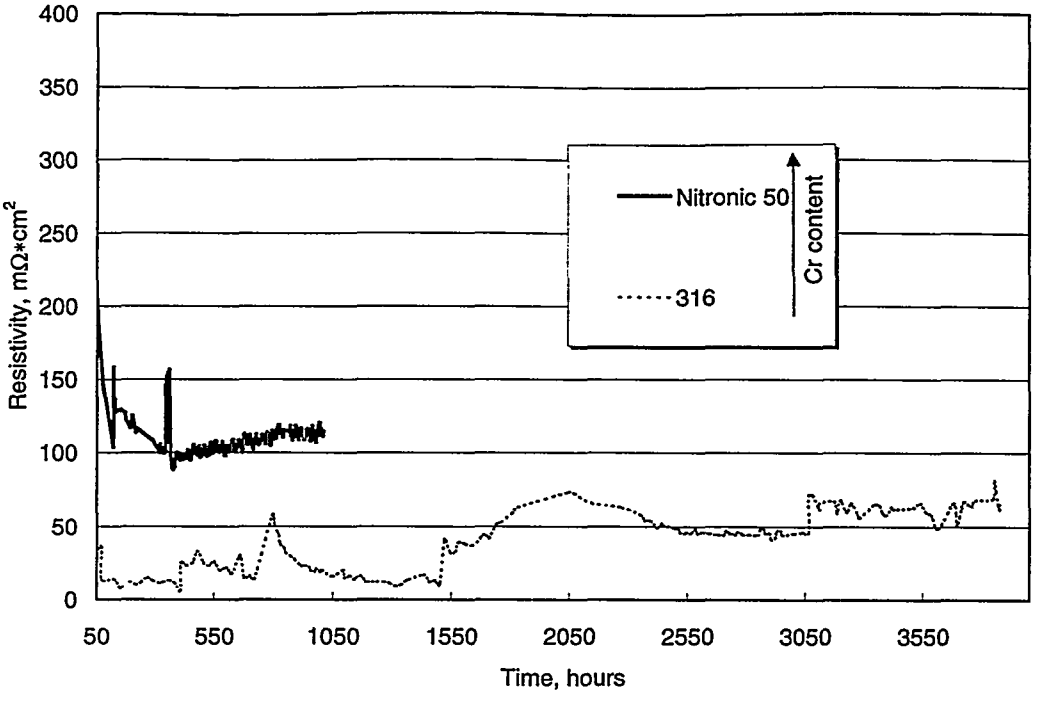

SUMMARY

The corrosion resistance of stainless steels under MCFC conditions is mainly influenced by the chromium content of the base metal. While the outer oxide scale of all analyzed stainless steels consists of $LiFeO_2$, the inner layer is strongly influenced by the chromium content of the base metal. The material 316L (chromium content <20 %) forms a structure such as $LiFe_5O_8$, where Cr is built in the structure or $LiFe_5O_8$ and $FeCrO_4$ coexist. The materials with Cr content >25% such as 310S and NKK have a $LiCrO_2$ inner layer. This layer is supposed to be a diffusion barrier for outward diffusion of iron cations, which explains the relatively thin oxides scales of 310S and NKK. Nitronic 50 has an improved corrosion resistance compared to 316L, which might be caused by the spinel supporting element Mn. The oxide scales of Nitronic 50 are modified with Mn.

The chemical composition of the electrolytes influences the oxide scale microstructure and the layer thickness as well. The (Li,Na) carbonate salt leads to dense scales without large cracks and spallation. This effect is attributed to the lower NiO dissolution rate under the less acidic (Li,Na) electrolyte.

The electrical conductivity of the oxides forming the scales determines the interfacial resistance. Indications show that the key factor is the phase composition of the inner layer. Both 310S and NKK have a $LiCrO_2$ inner layer, which probably causes the increased electrical resistivity, although the oxide scales are thin and compact. For NKK underlying porosity between the base metal and oxide scale is attributed to the increased resistivity compared to 310S.

A modified inner layer in Nitronic 50 may explain the improved conductivity of this material. Nitronic 50 seems to combine good corrosion resistance and low electrical resistivity and is a promising material for bipolar plates.

The oxide scale resistivity for 316L showed fluctuations over time. The change in oxide layer composition and oxide scale spallation/cracking for Type 316L samples is associated with transitions in interfacial resistivity. Examination of 316L oxide scale after 3000 h revealed formation of Ni/Fe oxide crystallites at its surface. The nickel component of the oxide scale is associated with lower resistance and gives support for lower resistance after 2000 h.

ACKNOWLEDGMENTS

This research was sponsored by the U.S. DOE Federal Energy Technology Center under Contract No. W-31-109-ENG-38. Tests and analytical work were supported by co op student participants: Carlos Centero, Edward Lee, Steve Nied, Michael Prescott, and Andrew Wagner.

REFERENCES

1. P. Biedenkopf, M. Spiegel, and H. J. Grabke, *Mater. and Corr.*, **48**, 477 (1997).

2. M. Keijzer, K. Hemmes, P. J. J. van der Put, J. H. W. de Wit, and J. Schoonman, *Corr. Sci.*, **39**, No. 3, 483 (1997).

3. M. S. Yaziki and J. R. Selman, in *Proc. of the Tenth Int. Symp. on Molten Salts*, R. T. Carlin, M. Matsunaga, J. R. Selman, S. Deki, D. S. Newman, and G. R. Stafford, Editors, PV 96-7, p. 423 The Electrochemical Society Proceedings, Pennington, NJ (1996).

4. M. Spiegel, P. Biedenkopf, and H. J. Grabke, *Corr. Sci.*, **39,** No.7,1193 (1997).

5. P. Biedenkopf, M. M. Bischoff, M. Spiegel, and H. J. Grabke, in *Proc. of the Fourth Int. Symp. on Carbonate Fuel Cell Technology*, J. R. Selman, I. Uchida, H. Wendt, D. A. Shores, T. F. Fuller, Editors, PV 97-4, p. 386, The Electrochemical Society Proceedings, Pennington, NJ (1997).

6. C. Y. Yuh, R. Johnson, M. Farooque, and H. Maru, in *Proc. of the Third Int. Symp. on Carbonate Fuel Cell Technology*, D. Shores, I. Uchida, H. Maru, J. R. Selman, Editors, PV 93-3, p. 158 The Electrochemical Society Proceedings, Pennington, NJ (1993).

7. B. Kim, H. Yoshitake, N. Kamiya, and K. Ota, in *Proc. of the Int. Symp. on Molten Salt Chemistry and Technology*, M.-L. Saboungi, and H. Kojima, Editors, PV 93-9, p. 321 The Electrochemical Society Proceedings, Pennington, NJ (1993).

8. W. A. Ghanem, *Steel Res.*, **64,** 317 (1993).

9. K. Ota, B. Kim, Y. Abi, H. Joshitake, and N. Kamiya, in *Proc. of the Third Int. Symp. on Carbonate Fuel Cell Technology*, D. Shores, I. Uchida, H. Maru, J. R. Selman, Editors, PV 93-3, p. 252 The Electrochemical Society Proceedings, Pennington, NJ (1993).

10. T. D. Kaun, I. D. Bloom and M. Krumpelt, *Proc. of the Fuel Cells '97 Review Meeting*, August 26-28, 1997, Vol.7-3, (1997).

11. C.Y. Yuh, C.M. Huang and M. Farroque, *Proc. of the Fourth Int. Symp. on Carbonate Fuel Cell Technology*, J. R. Selman, I. Uchida, H. Wendt, and D. Shores, T.F. Fuller, Editors, PV 97-4, p. 66, The Electrochemical Society Proceedings, Pennington, NJ (1997).